Effect of Al Doping on Magnetic Properties of Co-Mn Nanoferrites Synthesized *via* Citrate-Gel Method

Shankar Barapati[1,], M. Raghasudha[2,*,] and P. Veera Somaiah[1,*]

[1]Department of Chemistry, University College of Science, Osmania University, Hyderabad-500007, India
[2]Department of Chemistry, National Institute of Technology Warangal, Warangal-506004, India

*Corresponding authors: E-mail: raghas13chem@nitw.ac.in; vs_puppala@rediffmail.com

The structural and magnetic properties of aluminium substituted Co-Mn nanoferrites synthesized *via* a chemical route *viz*. citrate-gel autocombustion method have been reported. Aluminium content has been varied from $x=0$ to $x=1$ with an increment of 0.2 in $Co_{0.75}Mn_{0.25}Al_xFe_{2-x}O_4$. The structural confirmation was done with the basic characterization techniques such as XRD study, FTIR spectroscopic and the surface morphology was examined using SEM and EDX spectroscopic analysis. To study the optical absorption behaviour of the prepared ferrites, UV-visible spectral analysis was carried out. XRD analysis established the formation of cubic spinel structure of the materials with the average crystallite size of 15.5 nm to 19.94 nm. FTIR spectra has shown two absorption peaks that are characteristic of spinel nano ferrites. From the UV-visible spectral data, energy band gap (E_g) values were evaluated. The data witnessed an increase in the E_g value of the ferrite by doping of Al^{3+} ion into the ferrite. Room temperature magnetization measurements were carried out before and after aluminium doping in the samples using vibrating sample magnetometer. It was revealed that the substitution of aluminium in the lattice has modified the material into a soft magnetic material. Consequently, they find applications in transformer and motor cores.

Keywords: Nanoferrites, Citrate-gel, Autocombustion method, Magnetization measurements.

INTRODUCTION

Nanoferrites are the ceramic ferrimagnetic materials with iron oxides as their principal component that can be partially modified by the transition metal oxides. Based on the crystalline structure, ferrites are categorized into hexagonal ($MFe_{12}O_{19}$), garnets ($M_3Fe_5O_{12}$) and spinels (MFe_2O_4), where M stands for bivalent transition metal (*e.g.* Fe, Co, Ni, Cu, Zn and Mn) [1]. Synthesis of spinel nanoferrites has allured the attention of scientific community owing to their versatile technological applications in electronic devices, biomedical field and catalysis area [2,3]. Spinel nanoferrites also have some intriguing properties such as extreme stability over a wide range of pH, insolubility in most of the solvents, heterogeneity, remarkable magnetic properties, simplistic method of synthesis. These properties make them to use in diverse fields such as catalysis. Characteristic feature of any catalyst is it's easy recovery and reusability. Owing to their extraordinary magnetic properties, there is a greater demand for spinel nanoferrites as catalysts. Spinel nanoferrites can be easily recovered using an external magnet [4]. Due to noteworthy magnetic and dielectric properties, spinel nanoferrites are used as microwave absorbing materials that comprise of dielectric and magnetic materials [5].

Spinel ferrites are the most fascinating magnetic materials generally represented as $M^{2+}(Fe_2^{3+}O_4)$ where $M^{2+} = Mn^{2+}$, Co^{2+}, Cu^{2+}, Ni^{2+}, Zn^{2+}, *etc*. ions can reside either in tetrahedral (A) or octahedral (B) interstitial sites. Oxygen has fcc close packing arrangement [6]. The structure of spinel nanoferrites facilitate the exposure of octahedral (B) sites upon the surface and the presence of the tetrahedral (A) sites in the bulk. It is a well-known fact that catalysis is a surface process. Hence, M^{n+} ions located in the octahedral sites are greatly accountable for the catalytic effect by spinel nanoferrites. It is clear fact that the structure and nature of metal ion present at different sites in structure are responsible for the efficiency of catalytic activity of spinel ferrites. The metal ions at octahedral sites are placed

at relatively large distances thus provide ample space for the reactant molecules to interact in a facile way [7].

Among the various spinel ferrites $MnFe_2O_4$ and $CoFe_2O_4$ are very significant materials due to their distinctive features. $MnFe_2O_4$ are characterized into soft magnetic materials possessing high magnetic permeability and low losses. $MnFe_2O_4$ has gained appreciable attention because of its varied range of applications in various technological fields, which includes high frequency transformers, microwave electronic devices, computer memories, magnetic recording media and high-density information storage [8]. They are specifically identified for the use in biomedical applications, introducing into tumour tissues and drug delivery and catalysis [9]. On the other hand, $CoFe_2O_4$ is another promising magnetic material, which have gained extensive importance on account of its high electro-magnetic behaviour apart from its outstanding chemical stability and excellent mechanical hardness. $CoFe_2O_4$ is used in high density recording media owing to its good saturation magneti-zation and coercivity and powerful anisotropy [10].

Substitution of metal ions in spinel nanoferrites is an exce-llent approach for enhancing the desired properties for a specific application [11]. In view of this, many researchers have reported the enhancement of the properties of spinel nanoferrites by doping with various metal ions. Palamaru *et al*. [12] reported the synthesis and characterization of $CoMn_xFe_{2-x}O_4$ by combustion method. They have observed an increase in saturated magnetization with an increase in Mn content. Kim *et al*. [13] reported the investigation of structural and magnetic properties of manganese substituted cobalt ferrites prepared by sol-gel combustion [13]. Ahalya *et al*. [14] reported the effect of Co substitution on adsorption efficiency towards Cr(VI). Carlos Fernandes *et al*. [15] have studied the impact of substitution between Mn(II), Co(II) and the effect of the alkaline agent on the morphological properties and magnetic, chemical prop-erties of the nanomaterials. Javed *et al*. [16] have synthesized and studied the structural, dielectric and electrical properties of $Co_{1-x}Mn_xFe_2O_4$ prepared by chemical co-precipitation technique.

To tailor the properties of Co-Mn nanoferrites for a desired application, few researchers have reported doping of some metal ions into these ferrites. Fadafan *et al*. [17] have reported the thermoelectric powder and dielectric studies of Co-Mn-Zn nanoferrites [17]. Many researchers have reported the effect of introducing the transition metal ions and rare-earth metal ions into $CoFe_2O_4$ and $MnFe_2O_4$ on their properties [18-21]. Nevertheless, the effect of *p*-block elements on various properties of Co-Mn nanoferrites was seldom considered by researchers. Among various *p*-block elements (*e.g*. Al, In, Sn, Ga and Bi), Al doping has resulted in a smaller particle size and also octa-hedral site preference. On account of smaller ionic size of Al, a decrease in particle size is expected by incorporating Al ion in lattice of spinel nanoferrites [4]. Thus, surface area will be increased resulting in the enhancement of various properties and catalytic efficiency will also be expected to increase. Hence, Aluminium incorporated Co-Mn spinel nanoferrites has been undertaken for the study in the current work. The present work reports the synthesis of Co-Mn-Al nanoferrites and their elec-

trical and magnetic properties. Distribution of M^{n+} ions among the tetrahedral and octahedral sites and the crystallite size greatly influence the properties of ferrites. They are also influenced by the method of synthesis.

The literature reports various methods for the preparation of spinel nanoferrites such as co-precipitation method, hydro-thermal method, ball milling method, micro-emulsion method, reverse micelle method, thermal decomposition method, sol-gel autocombustion method, *etc*. [22,23]. Even though, expected microstructure and particles size are attained by using these methods, they are associated with complex procedures, high reaction temperature, very long reaction times, potentially harm-ful byproducts and toxic reagents [23]. Out of various synthesis methodologies, the facile, viable and efficient method, which produces spinel nanoferrites with good purity at a low reaction temperature and has a great control on the size of the particle, chemical composition and morphology is sol-gel method [24]. Sol-gel method is associated with generation of heat and redox reaction of xerogel. This gel is formed from aqueous solution consisting of required metal salts which act as oxidizers and organic complexant that acts as reductant. In the course of the combustion of xerogel, instantaneous release of large volume of gases results in the development of nanoparticles. Hence, in the present work, the facile sol-gel auto-combustion method is adopted for the synthesis of Co-Mn-Al spinel nanoferrites under investigation. Study of magnetic and electrical properties of the synthesized ferrites was carried out in the present work.

EXPERIMENTAL

Characterization: The structural characterization of the synthesized $Co_{0.75}Mn_{0.25}Al_xFe_{2-x}O_4$ nanoferrite samples was carried out at room temperature by X-ray diffractometer using Cu$K\alpha$ radiation (λ = 1.5405 Å) by scanning in the range of 10° to 80°, where the phase and crystallite size were investi-gated. The surface morphology of the prepared nanoferrite samples and their average particle size was analyzed by scanning electron microscope (SEM). Energy dispersive spectrometer (EDS) was used for elemental analysis of the samples. The FTIR absorption spectra of powders (as pellets in KBr) were recorded by Fourier transform infrared spectrophotometer in the range of 4000-200 cm^{-1}. Room temperature magnetization studies were carried out using vibrating sample magnetometer.

Synthesis: The Co-Mn-Al nanoferrites with the chemical composition $Co_{0.75}Mn_{0.25}Al_xFe_{2-x}O_4$ (where *x* = 0.0, 0.2, 0.4, 0.6, 0.8, 1.0) were synthesized by citrate-gel autocombustion method. This combustion method is a quick and straight forward method to synthesize homogeneous, nanocrystalline and un-agglomerated ferrite powders without the intermediate. These samples were successfully synthesized at lower temperatures in comparison with the conventional high temperature sintering. In this method of preparation, citric acid is used as fuel and oxidant. An exothermic reaction takes place between the metal nitrates and citric acid where the enthalpy of the reaction was used to synthesize the material in the nanocrystalline form. Cobalt(II) nitrate hexahydrate ($Co(NO_3)_2 \cdot 6H_2O$, 98%), ferric nitrate nonahydrate ($Fe(NO_3)_3 \cdot 9H_2O$, 98%), manganese(II)

nitrate tetrahydrate ($Mn(NO_3)_2 \cdot H_2O$, 98%), aluminium nitrate nonahydrate ($Al(NO_3)_3 \cdot 9H_2O$, 98%), citric acid and ammonia solution (AR grade) obtained from Merck, India were used as preparatory materials for the synthesis of different compositions of proposed ferrites. In this method, molar ratio of metal nitrates to citric acid was fixed at 1:3. The calculated quantities of metal nitrates and citric acid were dissolved independently in little amount of deionized water at room temperature. All the resulting aqueous solutions were added together and positioned on a magnetic stirrer at 60-70 ℃ and stirred well until homogeneous solution is obtained. The pH of the solution is maintained at 7 by adding ammonia solution. During the process, citric acid behaves as a complexing agent which forms a complex and afford fuel for self-ignition. Heating was continued to 90-100 ℃ with continuous stirring resulting in the formation of brown viscous gel. On further heating, the gel get self-ignited impulsively and burnt with a large flame. The whole ignition process was carried out in ambient air where gaseous products were formed resulting in a loose fluffy powder of greyish brown ash [25]. The ash was grounded into fine powder form in agate mortar. The obtained dry powder of various compositions of Co-Mn-Al ferrites was subjected to calcination at 900 ℃ for 5 h in high temperature electrical muffle furnace at a heating rate of 10 ℃/min. The powders were cooled to room temperature and ground to result in nanoferrites of various compositions. These powders were subjected to the structural characterization and their properties were studied.

RESULTS AND DISCUSSION

X-ray diffraction studies: To confirm the phase formation and for microstructural studies, the X-ray powder diffraction analysis was carried out on the synthesized $Co_{0.75}Mn_{0.25}Al_xFe_{2-x}O_4$ nanoferrite powder samples. The X-ray diffraction patterns of the samples are indexed as (111), (220), (311), (400), (511), (440), (533) (Fig. 1a) with reference to the JCPDs card Nos. 20-1086 ($CoFe_2O_4$) and 74-2403 ($MnFe_2O_4$) [26]. It indicates the formation of cubic spinel structure of the ferrites with single phase without any impurity pickup. The enlarged 311 peak is shown in Fig. 1b, whereas, it is observed that the peak shifted towards the higher 2θ values, which may be ascribed to the decrease in lattice parameter.

The structural parameters of the samples *i.e.* crystallite size, lattice parameter and X-ray density were calculated. The crystallite size 'D' of the samples have been calculated from the full width at half maximum (FWHM) of the strongest reflection of the plane (311) using the Debye Scherer's equation [27].

$$\text{Crystallite size } D = \frac{0.94\lambda}{\beta\cos\theta} \qquad (1)$$

where λ = wavelength of X-ray; β = full width half maximum in radians; and θ = Brag's angle at peaks position.

The average crystalline size of the synthesized samples was in the range of 15.5-19.94 nm. A decrease in crystalline size was observed with increase in aluminium content. Lattice parameter (a) of the prepared ferrite samples was determined using the following formula:
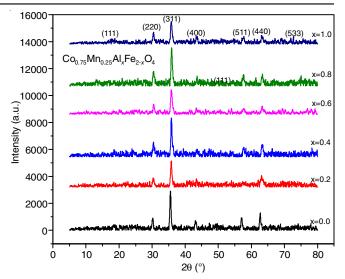

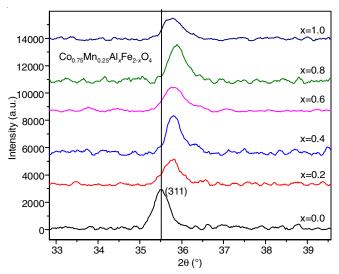Fig. 1a. X-ray diffraction patterns of $Co_{0.75}Mn_{0.25}Al_xFe_{2-x}O_4$ nanoferrites (0.0 ≤ x ≤ 1.0)

Fig. 1b. Enlarged 311 peaks for the $Co_{0.75}Mn_{0.25}Al_xFe_{2-x}O_4$ nanoferrite compositions

$$\text{Lattice parameter} = a = d\sqrt{h^2 + k^2 + l^2} \qquad (2)$$

where d = inter planar spacing; *hkl* = miller indices.

X-ray density (d_x) of the samples can be calculated using the following formula [28]:

$$\text{X-ray density} = d_x = \frac{8M}{Na^3}(g/cc) \qquad (3)$$

where M = Molecular weight of the sample; N = Avagadro number; a = lattice parameter

The calculated values of crystallite size, lattice parameter, X-ray density and volume of the unit cell for various compositions of Co-Mn-Al ferrites are tabulated in Table-1. It is clear that there is a decrease in the values of lattice parameter, X-ray density and volume of the unit cell the prepared Co-Mn-Al nanoferrites with increase in the Al content. The variation of lattice parameter with the aluminium content is shown in Fig. 2.

Morphological studies: Agglomeration of the prepared nanoparticles was realized from the SEM images and also the

TABLE-1
CRYSTALLITE SIZE (nm), LATTICE PARAMETER (Å), X-RAY DENSITY (d_x) (g/cc),
VOLUME OF THE UNIT CELL (Å)^3 of Co-Mn-Al FERRITES

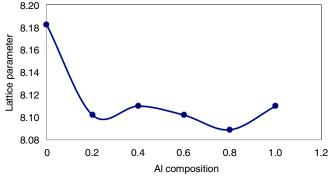| Al content (x)	Ferrite composition	Crystallite size (nm)	Lattice parameter (Å)	X-ray density (d_x) (g/cc)	Volume of the unit cell V = a^3 (Å)^3
0.0	$Co_{0.75}Mn_{0.25}Fe_2O_4$	19.94	8.182	5.65	547.74
0.2	$Co_{0.75}Mn_{0.25}Al_{0.2}Fe_{1.8}O_4$	19.07	8.102	5.68	531.86
0.4	$Co_{0.75}Mn_{0.25}Al_{0.4}Fe_{1.6}O_4$	19.80	8.110	5.52	533.78
0.6	$Co_{0.75}Mn_{0.25}Al_{0.6}Fe_{1.4}O_4$	15.09	8.102	5.40	531.86
0.8	$Co_{0.75}Mn_{0.25}Al_{0.8}Fe_{1.2}O_4$	17.80	8.089	5.28	529.30
1.0	$Co_{0.75}Mn_{0.25}AlFeO_4$	15.50	8.110	5.09	533.78

Fig. 2. Variation of lattice parameter with Al content in $Co_{0.75}Mn_{0.25}Al_xFe_{2-x}O_4$ ($0.0 \le x \le 1.0$)

surface morphology was similar as shown in Fig. 3. Agglomeration revealed that the distribution of the grain size is broad but not uniform. Broad size of the particle inferred the development of mechanically activated nanoparticles. The particles possess a permanent magnetic moment, which is directly related to their volume culminating in the agglomeration of particles. The EDS spectra of the Al doped Co-Mn nanoferrites are shown in Fig. 4. The EDS spectra confirms the presence of added Co, Mn, Al, Fe, O elements only and no impurity was observed in the samples.

FTIR studies: The FTIR spectra of the prepared ferrites were recorded in 3000-200 cm^{-1} at room temperature and are shown in Fig. 5. The two clear absorption bands v_1 and v_2 were observed at about 600 and 400 cm^{-1} which signify the intrinsic stretching vibrations of tetrahedral (A) and octahedral (B) sites, respectively [29]. The first absorption band at 626-570 cm^{-1} indicates the stretching vibration of tetrahedral M-O bond, while the other band detected in the range of 496-405 cm^{-1} results from the stretching vibrations of metal-oxygen band at octahedral site.
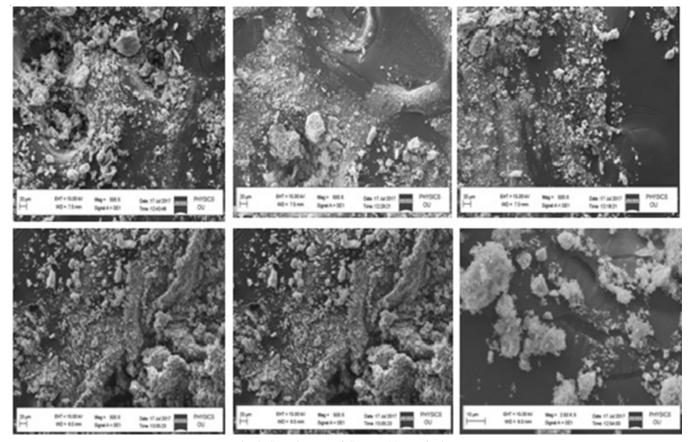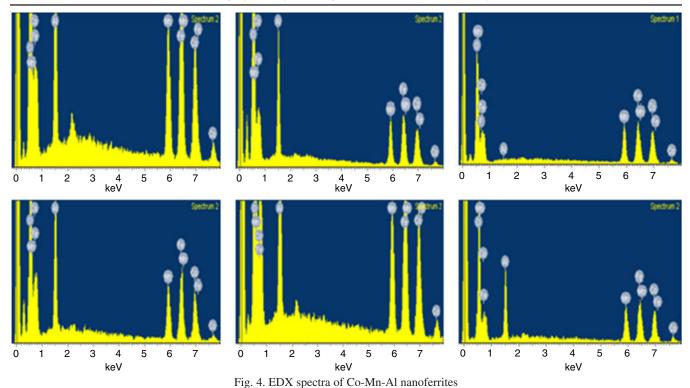

Fig. 3. SEM images of Co-Mn-Al nanoferrites

Fig. 4. EDX spectra of Co-Mn-Al nanoferrites

Fig. 5. FTIR spectra of $Co_{0.75}Mn_{0.25}Al_xFe_{2-x}O_4$ nanoferrites ($0.0 \leq x \leq 1.0$)

TABLE-2
FTIR PARAMETERS OF $Co_{0.75}Mn_{0.25}Al_xFe_{2-x}O_4$
NANOFERRITES ($0.0 \leq x \leq 1.0$)

Composition of ferrite	ν_1 (cm^{-1})	ν_2 (cm^{-1})
$Co_{0.75}Mn_{0.25}Fe_2O_4$	620	489
$Co_{0.75}Mn_{0.25}Al_{0.2}Fe_{1.8}O_4$	615	484
$Co_{0.75}Mn_{0.25}Al_{0.4}Fe_{1.6}O_4$	580	410
$Co_{0.75}Mn_{0.25}Al_{0.6}Fe_{1.4}O_4$	570	405
$Co_{0.75}Mn_{0.25}Al_{0.8}Fe_{1.2}O_4$	609	472
$Co_{0.75}Mn_{0.25}AlFeO_4$	626	496

UV-visible absorption studies: The UV-visible diffuse reflectance studies were carried out to study the effect of Al^{3+} ions doping in the Co-Mn nanoferrites. The optical absorption spectrum of $Co_{0.75}Mn_{0.25}Al_xFe_{2-x}O_4$ nanoferrites ($0.0 \leq x \leq 1.0$) in the range of 200 to 600 nm as shown in Fig. 6. Further, the band gap energy of the materials is computed from the optical reflectance data with the help of Tauc and Davis-Mott relation [32] given as:

$$(\alpha h\nu)^n = K(h\nu - E_g) \qquad (4)$$

where α = absorption coefficient, $h\nu$ = incident photon energy, K = energy independent constant, E_g = optical band gap energy of the nanomaterial, n = a constant indicative of the nature of transition [33] and for direct band gap of spinel ferrites, n = 2 [34].

Fig. 7 shows the Tauc plot of all the compositions of the ferrites where $(\alpha h\nu)^2$ was plotted against energy on *x*-axis. From the absorbance (A) data, α was calculated, while the energy in eV was calculated using the wavelength using eqn. 5:

$$\text{Energy} = \frac{1240}{\lambda} \qquad (5)$$

where λ is the wavelength of incident photon.

The vibrational spectra of ferrites were studied by Waldron [30] and Hafner [31] and ascribed the high frequency band (ν_1) at about 600 cm^{-1} to tetrahedral (A) site and low frequency band (ν_2) at about 400 cm^{-1} to octahedral (B) site. The observed absorption bands within these specific range indicated the formation of single phased spinel structure with two sub-lattices namely tetrahedral (A) site and octahedral (B) site. The variance between ν_1 and ν_2 is because of the differences in distances of positions of Fe^{3+} and O^{2-} at tetrahedral and octahedral sites. The values of absorption bands for various ferrite compositions are given in Table-2.
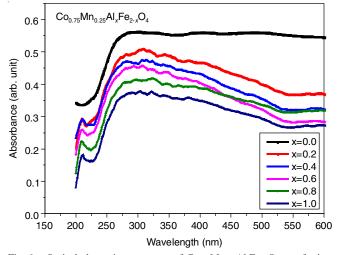
Fig. 6. Optical absorption spectrum of $Co_{0.75}Mn_{0.25}Al_xFe_{2-x}O_4$ nanoferrites $(0.0 \leq x \leq 1.0)$

Fig. 8. Tauc plot confirming the direct band gap ferrites

Fig. 8 confirms that the prepared ferrites are the direct band gap materials as the Tauc plot with $(\alpha h\nu)^2$ against energy shows linear part. The inset figure shows the Tauc plot with $(\alpha h\nu)^{0.5}$ against energy, which does not show any linear part thus confirmed no indirect allowed transition.

The energy gap (E_g) values from the Tauc plots as the intercepts of the linear absorption part on the energy axis (*x*-axis) where $(\alpha h\nu)^2$ is zero. The optical energy band gap values of various compositions of Co-Mn-Al nanoferrites are tabulated in Table-3. The energy band gap values infer that doping of Al in Co-Mn nanoferrites has resulted in an increase in the energy band gap of the material. The variation of energy band gap with Al doping is shown in Fig. 9.

Magnetization measurements: The magnetic properties of the $Co_{0.75}Mn_{0.25}Al_xFe_{2-x}O_4$ nanoferrites were evaluated with
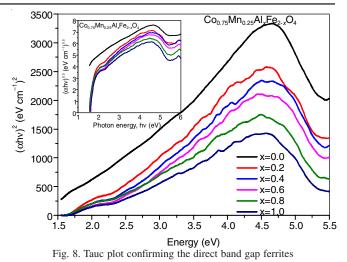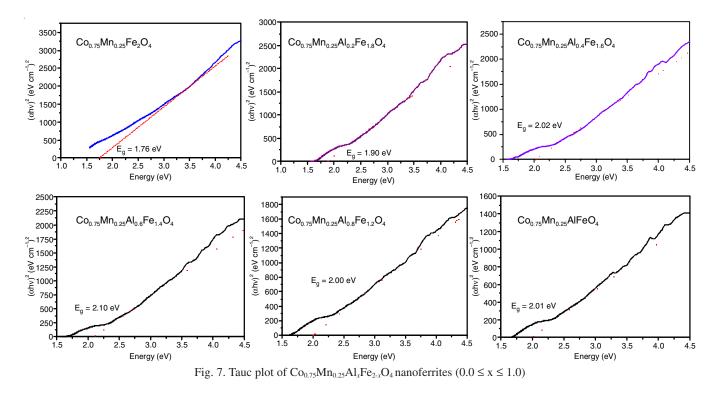
TABLE-3 OPTICAL ENERGY BAND GAP VALUES OF VARIOUS COMPOSITIONS OF Co-Mn-Al NANOFERRITES	
Composition of ferrite	Band gap energy (eV)
$Co_{0.75}Mn_{0.25}Fe_2O_4$	1.76
$Co_{0.75}Mn_{0.25}Al_{0.2}Fe_{1.8}O_4$	1.90
$Co_{0.75}Mn_{0.25}Al_{0.4}Fe_{1.6}O_4$	2.02
$Co_{0.75}Mn_{0.25}Al_{0.6}Fe_{1.4}O_4$	2.10
$Co_{0.75}Mn_{0.25}Al_{0.8}Fe_{1.2}O_4$	2.00
$Co_{0.75}Mn_{0.25}AlFeO_4$	2.01

the help of vibrating sample magnetometer. The room temperature magnetization measurements of pure Co-Mn nanoferrite and Al doped Co-Mn nanoferrites were studied in 5 kOe. Fig. 10 shows the magnetization hysteresis curves for the pure and Al substituted nanoferrites. The magnetic parameters extracted from the individual hysteresis loops of the pure and Al doped Co-Mn nanoferrite samples are tabulated in Table-4.
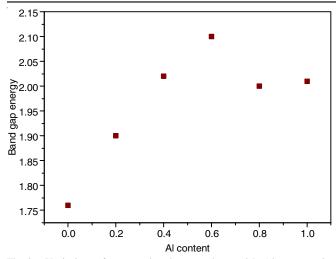

Fig. 7. Tauc plot of $Co_{0.75}Mn_{0.25}Al_xFe_{2-x}O_4$ nanoferrites $(0.0 \leq x \leq 1.0)$

Fig. 9. Variation of energy band gap values with Al content in $Co_{0.75}Mn_{0.25}Al_xFe_{2-x}O_4$

TABLE-4
MAGNETIC PARAMETERS OF
$Co_{0.75}Mn_{0.25}Al_xFe_{2-x}O_4$ FERRITES ($x = 0.0$ AND 0.2)

Ferrite composition	H_c	M_s	M_r	$S = M_r/M_s$
$Co_{0.75}Mn_{0.25}Fe_2O_4$	164.945	0.890	0.248	0.279
$Co_{0.75}Mn_{0.25}Al_{0.2}Fe_{1.8}O_4$	38.149	0.249	0.030	0.123

The observed decline in the values of all magnetic parameters with rise in aluminium content in the ferrite lattice may perhaps be due to the weakening of A-B super exchange interactions owing to the replacement of Fe^{3+} ions by Al^{3+} ions at octahedral [B] sites [4,35]. The magnetization value declined with rise in Al content as expected and also reported by Singh *et al*. [36].

A steep fall in saturation magnetization is ascribed to the presence of some degree of spin canting in the bulk volume of nanoparticles. Spin canting is a phenomenon through which the spins are slightly tilted about their axis by a small angle than being present exactly co-parallel. The other fact that influ-ences the saturation magnetization is strength of exchange inter-actions. Trivalent aluminium ion does not possess any magnetic moment due to zero unpaired electrons. When Al^{3+} ion replaces some of the Fe^{3+} ions, the magnetic coupling weakens resulting in weakening of A-B exchange interactions. Thus, it results in the disturbance of spin ordering, consequently the magnetic ordering is destabilized. The Al^{3+} ions (zero magnetic moment) have the octahedral site preference which replaces the magnetic Fe^{3+} ions (magnetic moment 5 µB). Hence, as Al^{3+} is doped in Co-Mn ferrite, it results in a decrease in Fe^{3+} (B):Fe^{2+} (B) ratio and thus weakening of A-B exchange interaction [37].

It is clear that substitution of non-magnetic aluminium ions for magnetic Fe^{3+} ions consequences in decrease in all the magnetic parameters indicating the fact that the material has been transformed into a soft magnetic material by the sub-stitution of aluminium ions. Hysteresis loops assist to differen-tiate soft and hard magnetic materials. For a hard-magnetic material, the part inside the hysteresis curve is huge, which signifies the quantity of useful magnetic energy that is made accessible to carry out work. Whereas, for a soft magnetic material, the part inside the loop is so little that a very minimum amount of dissipated energy is repetitively reversing the magne-tization. Hysteresis loops obtained for the pure Co-Mn ferrites and Al doped Co-Mn ferrites in the present work indicate that the area inside the loop for pure Co-Mn ferrite is more when compared to that of Al doped Co-Mn ferrite. This confirms the fact that aluminium substitution has made the Co-Mn ferrite sample magnetically very soft material.

Conclusion

$Co_{0.75}Mn_{0.25}Al_xFe_{2-x}O_4$ (where $x = 0.0$, 0.2, 0.4, 0.6, 0.8, 1.0) nanoferrites were successfully synthesized *via* citrate-gel autocombustion method. The X-ray diffraction analysis con-firmed the formation of cubic spinel structure with a particle size ranging from 15.5-19.9 nm. The SEM images confirmed the agglomeration of the particles in the sample and also the EDS analysis indicates no impurity pickup in the sample. The
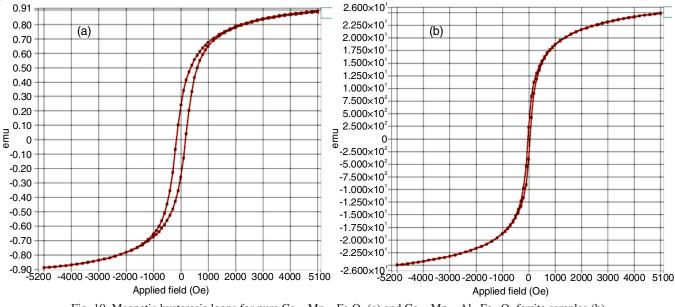

Fig. 10. Magnetic hysteresis loops for pure $Co_{0.75}Mn_{0.25}Fe_2O_4$ (a) and $Co_{0.75}Mn_{0.25}Al_{0.2}Fe_{1.8}O_4$ ferrite samples (b)

FTIR analysis confirmed the formation of cubic spinel structure of the samples. The optical absorption behaviour shows that the prepared ferrites are the direct band gap materials in which the Al doping has increased the band gap energy of Co-Mn nanoferrites. The magnetization study of the sample at room temperature indicates the magnetic behaviour of the samples. Aluminium doping in the Co-Mn nanoferrite sample has changed the material into a magnetically very soft material that can find applications in transformer and motor cores.

CONFLICT OF INTEREST

The authors declare that there is no conflict of interests regarding the publication of this article.

REFERENCES

1. B.I. Kharisov, H.V. Rasika Dias and O.V. Kharissova, *Arab. J. Chem.*, **12**, 1234 (2019);
https://doi.org/10.1016/j.arabjc.2014.10.049

2. E. Karaoglu and A. Baykal, *J. Supercond. Nov. Magn.*, **27**, 2041 (2014);
https://doi.org/10.1007/s10948-014-2522-3

3. A.A. Dakhel, M. El-Hilo and M. Bououdina, *J. Supercond. Nov. Magn.*, **27**, 2089 (2014);
https://doi.org/10.1007/s10948-014-2553-9

4. A. Goyal, S. Bansal, B. Chudasama, K.B. Tikoo, V. Kumar and S. Singhal, *New J. Chem.*, **41**, 8320 (2017);
https://doi.org/10.1039/C7NJ01486D

5. A. Teber, K. Cil, T. Yilmaz, B. Eraslan, D. Uysal, G. Surucu, A.H. Baykal and R. Bansal, *Aerospace*, **4**, 2 (2017);
https://doi.org/10.3390/aerospace4010002

6. A. Manikandan, M. Durka and S.A. Antony, *J. Supercond. Nov. Magn.*, **27**, 2841 (2014);
https://doi.org/10.1007/s10948-014-2771-1

7. V.S. Kiran and S. Sumathi, *J. Magn. Magn. Mater.*, **421**, 113 (2017);
https://doi.org/10.1016/j.jmmm.2016.07.068

8. H. Naeimi, Z. Rashid, A.H. Zarnani and R. Ghahremanzadeh, *New J. Chem.*, **38**, 5527 (2014);
https://doi.org/10.1039/C4NJ01182A

9. M. Hesampour, M. Ali Taher and M. Behzadi, *New J. Chem.*, **41**, 12910 (2017);
https://doi.org/10.1039/C7NJ01742A

10. C. Cheng, J. Dai, Z. Li and W. Feng, *Materials*, **13**, 3860 (2020);
https://doi.org/10.3390/ma13173860

11. C.Y. Tsay, Y.C. Chiu and C.M. Lei, *Materials*, **11**, 2274 (2018);
https://doi.org/10.3390/ma11112274

12. M.N. Palamaru, A.R. Iordan, C.D. Aruxandei, I.A. Gorodea, E.A. Perianu, I. Dumitru, M. Feder and O.F. Caltun, *J. Optoelectr. Adv. Mater.*, **10**, 1853 (2008).

13. W.C. Kim, Y.S. Yi and C.S. Kim, *J. Magn. (Korea)*, **5**, 111 (2000).

14. K. Ahalya, N. Suriyanarayanan and V. Ranjith Kumar, *J. Magn. Magn. Mater.*, **372**, 208 (2014);
https://doi.org/10.1016/j.jmmm.2014.07.030

15. C. Fernandes, C. Pereira, M.P. Fernandez-Garcia, A.M. Pereira, A. Guedes, R. Fernandez-Pacheco, A. Ibarra, M.R. Ibarra, J.P. Araújo and C. Freire, *J. Mater. Chem. C Mater. Opt. Electron. Devices*, **2**, 5818 (2014);
https://doi.org/10.1039/C4TC00429A

16. T. Javed, A. Maqsood and A.A. Malik, *J. Supercond. Nov. Magn.*, **24**, 2137 (2011);
https://doi.org/10.1007/s10948-011-1168-7

17. H.K. Fadafan, S. Nezhadeini and P. Lotfalinezhad, *J. Supercond. Nov. Magn.*, **33**, 2037 (2020);
https://doi.org/10.1007/s10948-020-05459-5

18. W. Wang, Z. Ding, S. Wu, F. Li and J. Ping Liu, *Ceram. Int.*, **41**, 13624 (2015);
https://doi.org/10.1016/j.ceramint.2015.07.159

19. X.C. Zhong, X.J. Guo, S.Y. Zou, H.Y. Yu, Z.W. Liu, Y.F. Zhang and K.X. Wang, *AIP Adv.*, **8**, 047807 (2018);
https://doi.org/10.1063/1.4993645

20. A.B. Naik, P.P. Naik, S.S. Hasolkar and D. Naik, *Ceram. Int.*, **46**, 21046 (2020);
https://doi.org/10.1016/j.ceramint.2020.05.177

21. S. Iqbal, M. Fakhar-e-Alam, M. Atif, N. Amin, K.S. Alimgeer, A. Ali, A. Ul Ahmad, A. Hanif and A. Farooq, *Results Phys.*, **15**, 102529 (2019);
https://doi.org/10.1016/j.rinp.2019.102529

22. O. Perales-Perez and Y. Cedeno-Mattei, Magnetic Spinels-Synthesis, Properties and Application, Intech Open, pp. 51-72 (2016).

23. S. Jauhar, J. Kaur, A. Goyal and S. Singhal, *RSC Adv.*, **6**, 97694 (2016);
https://doi.org/10.1039/C6RA21224G

24. L. Wang, M. Lu, Y. Liu, J. Li, M. Liu and H. Li, *Ceram. Int.*, **41**, 4176 (2015);
https://doi.org/10.1016/j.ceramint.2014.12.099

25. M. Raghasudha, D. Ravinder and P. Veerasomaiah, *Adv. Mater. Lett.*, **4**, 910 (2013);
https://doi.org/10.5185/amlett.2013.5479

26. S.P. Yadav, S.S. Shinde, A.A. Kadam and K.Y. Rajpure, *J. Semicond.*, **34**, 093002 (2013);
https://doi.org/10.1088/1674-4926/34/9/093002

27. B.D. Cullity, Elements of X-ray diffraction, Addison Wesley Publishing Company, ed.: 3 (1976).

28. R.C. Kambale, P.A. Shaikh, S.S. Kamble and Y.D. Kolekar, *J. Alloys Compd.*, **478**, 599 (2009);
https://doi.org/10.1016/j.jallcom.2008.11.101

29. M. Kurian and D.S. Nair, *J. Saudi Chem. Soc.*, **20**, S517 (2016);
https://doi.org/10.1016/j.jscs.2013.03.003

30. R.D. Waldron, *Phys. Rev.*, **99**, 1727 (1955);
https://doi.org/10.1103/PhysRev.99.1727

31. S. Hafner, *Z. Kristallogr. Cryst. Mater.*, **115**, 331 (1961);
https://doi.org/10.1524/zkri.1961.115.5-6.331

32. A. Lassoued, M.S. Lassoued, B. Dkhil, S. Ammar and A. Gadri, *J. Mater. Sci. Mater. Electron.*, **29**, 7057 (2018);
https://doi.org/10.1007/s10854-018-8693-0

33. J.I. Pankov, Optical Processes in Semiconductors, Prentice-Hall Inc.: New Jercey, pp 31-34 (1971).

34. M. Mohammadikish, *Ceram. Int.*, **40**, 1351 (2014);
https://doi.org/10.1016/j.ceramint.2013.07.016

35. H.M. Zaki, S.H. Al-Heniti and A. Hashhash, *J. Magn. Magn. Mater.*, **401**, 1027 (2016);
https://doi.org/10.1016/j.jmmm.2015.11.021

36. N. Singh, A. Agarwal, S. Sanghi and P. Singh, *J. Magn. Magn. Mater.*, **323**, 486 (2011);
https://doi.org/10.1016/j.jmmm.2010.09.053.

37. I.H. Gul and A. Maqsood, *J. Alloys Compd.*, **465**, 227 (2008);
https://doi.org/10.1016/j.jallcom.2007.11.006